Published in final edited form as:
Angew Chem Int Ed Engl. 2012 July 9; 51(28): 6908–6911. doi:10.1002/anie.201201690.

Cyclic Caged Morpholinos: Conformationally Gated Probes of Embryonic Gene Function**

Dr. Sayumi Yamazoe,
Departments of Chemical and Systems Biology and Developmental Biology, Stanford University School of Medicine, 269 Campus Drive, CCSR 3155, Stanford, CA 94305 (USA), Fax: (+1) 650-723-2253

Dr. Ilya A. Shestopalov,
Departments of Chemical and Systems Biology and Developmental Biology, Stanford University School of Medicine, 269 Campus Drive, CCSR 3155, Stanford, CA 94305 (USA), Fax: (+1) 650-723-2253

Dr. Elayne Provost,
Departments of Surgery, Oncology, and Cell Biology, McKusick-Nathans Institute of Genetic Medicine, Johns Hopkins University, 733 N. Broadway, BRB 471, Baltimore, MD 21205 (USA)

Prof. Dr. Steven D. Leach, and
Departments of Surgery, Oncology, and Cell Biology, McKusick-Nathans Institute of Genetic Medicine, Johns Hopkins University, 733 N. Broadway, BRB 471, Baltimore, MD 21205 (USA)

Prof. Dr. James K. Chen
Departments of Chemical and Systems Biology and Developmental Biology, Stanford University School of Medicine, 269 Campus Drive, CCSR 3155, Stanford, CA 94305 (USA), Fax: (+1) 650-723-2253, Homepage: http://chen.stanford.edu

James K. Chen: jameschen@stanford.edu

Keywords

Antisense oligonucleotides; Caged compounds; Gene expression; Zebrafish; Developmental biology

Deciphering the molecular mechanisms that underlie embryogenesis requires an ability to alter gene function with spatial and temporal precision. Synthetic reagents can be valuable tools in this discovery process, especially in model organisms currently intractable to targeted genomic changes. In particular, morpholino-based antisense oligonucleotides (MOs) have been widely used to inhibit gene expression in metazoans that develop *ex utero* (Figure 1a),[1–4] and caged versions of these reagents (cMOs) can enable conditional gene silencing through targeted illumination.[5–9] Composed of morpholino-based nucleosides and a phosphorodiamidate backbone, these nuclease-resistant probes are typically injected into zygotes as 25-base oligomers, after which they hybridize to complementary RNAs and disrupt splicing or translation. While cMOs can provide important new insights into embryonic gene function, their utility has been hindered by their empirical design, synthetic complexity, *in vivo* instability, reliance on complementary inhibitors, and/or use of multiple

**We thank A. Puri and I. Hinkson for their assistance. This work was supported by the NIH (R01 GM087292 and DP1 OD003792 to J. K. C.; R01 DK061215 to S. D. L.)

Correspondence to: James K. Chen, jameschen@stanford.edu.

caging groups. Here we describe next-generation cMOs that overcome these limitations. We demonstrate that cyclic cMOs are effective reverse-genetic tools in zebrafish embryos, and we use these reagents to examine the timing of exocrine fate commitment in the developing pancreas.

We previously developed hairpin cMOs that can be activated with either ultraviolet (UV; 360-nm) or two-photon irradiation (Figure 1b).[5, 10] The RNA-targeting MO is tethered to a shorter, complementary MO inhibitor through a dimethoxynitrobenzyl (DMNB)- or bromohydroxyquinoline (BHQ)-based linker, thereby forming a hairpin structure that is resistant to RNA hybridization. Linker photolysis separates the two oligonucleotides, allowing the 25-base MO to interact with its RNA target. Hairpin cMOs have been used to conditionally inactivate the expression of several zebrafish genes, including *no tail-a* (*ntla*), *floating head* (*flh*), *heart of glass* (*heg*), and *ETS1-related protein* (*etsrp*).[5, 10] We have also integrated *ntla* cMOs, caged fluorophores, fluorescence-activated cell sorting, and microarray technologies to dynamically profile the Ntla-dependent transcriptome.[11] Despite these successes, hairpin cMOs have limitations. Their design involves careful optimization of thermodyamic properties, their purification requires high-performance liquid chromatography (HPLC), and the inhibitory oligonucleotide can exacerbate MO toxicity.

Other oligonucleotide caging strategies have been developed, each with its own advantages and disadvantages. For example, peptide nucleic acid (PNA)-2-OMe RNA chimeras that form hairpins have been used to conditionally inhibit gene function,[6] although the photo-released 2-OMe RNAs may be toxic to embryos.[7] Duplexes composed of the targeting MO and two complementary, tandem oligonucleotides connected by a nitrobenzyl-based linker have also been reported (Figure 1c).[7, 9] While these duplexes are easier to prepare than hairpin reagents, they release two potentially cytotoxic oligonucleotides upon photolysis and can be less stable *in vivo*. Finally, MOs containing four nitropiperonyloxymethyl-caged thymine bases have been synthesized, bypassing the need for an inhibitory oligomer (Figure 1d).[8] Activating these reagents, however, requires the photolysis of multiple caging groups per oligonucleotide, which can be difficult to achieve without damaging levels of UV irradiation.

To overcome these limitations, we sought to develop cMOs that are easier to synthesize, rely on a single caging group, and do not involve a complementary inhibitor. Since oligonucleotide duplexes have limited tolerance for local curvature,[12] we hypothesized that MO cyclization through a photocleavable linker could enable conditional gene silencing (Figure 1e). A recent report that circular DNA oligonucleotides bind inefficiently to their complementary RNAs *in vitro* lends further support to this concept.[13]

We tested this new caging strategy by targeting *ntla*, the zebrafish ortholog of mammalian *Brachyury*.[14–16] Loss-of-function phenotypes for this T-box transcription factor include ablation of the notochord and posterior mesoderm, ectopic medial floor plate cells, and somite mispatterning. We synthesized a DMNB-functionalized linker with *N*-hydroxysuccinimide ester and chloroacetamide groups (Scheme 1) and reacted it with a 25-base *ntla* MO (Table S1) bearing 5′-amine and 3′-alkyl disulfide modifications (Scheme 1). Reduction of the linear MO-linker intermediate yielded the free thiol, which spontaneously reacted with the chloroacetamide to provide the desired macrocycle. Liquid chromatography-mass spectrometry (LCMS) analysis indicated that the macrocyclization reaction went to completion, and the final product was purified by gel filtration. The total yield for the 25-base cyclic *ntla* cMO synthesis starting with the linker and the targeting MO was 80%, approximately a 10-fold improvement over our hairpin cMO protocol.[10]

We next investigated the efficacy of the cyclic *ntla* cMO in zebrafish embryos. Since we had previously shown that the conventional, linear *ntla* MO recapitulates the *ntla* mutant phenotype at a dose of 1 ng/embryo,[5, 10] we delivered an equivalent amount of the photocleavable cyclic *ntla* cMO into zygotes and globally irradiated a subset of the embryos with UV light for 10 seconds at 3 hours post fertilization (hpf).[15] The embryos were cultured until 24 hpf, at which point their phenotypes were scored according to four morphological classes as previously described (Figure 2a).[10] The cyclic *ntla* cMO proved to be comparable to the hairpin reagent in terms of efficacy, if not modestly better, with approximately 75% (n=24) of the cMO-injected embryos exhibiting no developmental defects in the absence of UV light and 90% (n=20) achieving complete *ntla* mutant phenotypes upon UV irradiation (Figure 2b). Western blot analysis of 10-hpf zebrafish confirmed the UV light-dependent loss of Ntla protein in cyclic *ntla* cMO-injected embryos (Figure 2c). The cyclic *ntla* cMO could also be used to knockdown *ntla* function in a spatially restricted manner; photoactivation of the reagent within the embryonic shield at 6 hpf converted notochord progenitors into medial floor plate cells, as has been reported with hairpin *ntla* cMOs (Figure 2d).[5, 11]

In principle, the basal activity of cyclic cMOs should decrease with macrocycle size, as local curvature within the smaller MO macrocycles will be more acute. To explore this possibility, we synthesized non-photocleavable cyclic MOs corresponding to 21-, 23-, and 25-base oligonucleotides that target the *ntla* sequence (Table S1 and Scheme S1). The cyclic oligonucleotides or the corresponding linear MOs were then mixed with equimolar amounts of 25-base complementary RNA (Table S1), and temperature-dependent changes in hypochromicity were assessed (Table 1). Although these in vitro assays cannot recapitulate the complexity of MO/RNA interactions *in vivo*, the thermodynamic insights they provide can be informative.[10] As expected, the cyclic MOs exhibited reduced affinities for their RNA targets than their linear counterparts, and greater differences in T_m and ΔG values were observed as MO length decreased.

We next tested photoactivatable versions of these cyclic MOs and their linear counterparts in zebrafish embryos. As before, we globally UV-irradiated a subset of the cMO-injected embryos at 3 hpf and evaluated their morphological phenotypes at 24 hpf and Ntla protein levels at 10 hpf. Although the cyclic *ntla* cMOs exhibited less basal activity as they decreased in size, they also had a commensurate loss of efficacy upon uncaging (Figure 2, b–c). Linear versions of the 21- and 23-base reagents were similarly less potent, indicating that this activity reduction is due to diminished MO/RNA interactions. Thus, within this dosing regimen, the 25-base cyclic cMO appears to provide the optimum dynamic range of caged and uncaged activities.

To explore the generality of cyclic cMOs, we synthesized a 25-base reagent targeting *pancreas transcription factor 1 alpha* (*ptf1a*) (Table S1), which is required for exocrine cell differentiation in the developing pancreas.[17–19] Ptf1a is selectively expressed in pancreatic exocrine cells, and their formation can therefore be directly visualized in transgenic zebrafish that express enhanced green fluorescent protein under control of *ptf1a* promoter-derived *cis*-regulatory elements [*Tg*(*ptf1a:eGFP*) zebrafish].[20] We injected *Tg*(*ptf1a:eGFP*) zygotes with the cyclic *ptf1a* cMO at a dose of 2 ng/embryo and globally UV-irradiated a subset at 3 hpf for 10 seconds. Another set of *Tg*(*ptf1a:eGFP*) zygotes were injected with an equivalent amount of a hairpin *ptf1a* cMO that was designed according to thermodynamic parameters.[10] The intensity of eGFP fluorescence within the pancreatic field at 3 days post fertilization (dpf) was then scored for each experimental condition (Figure 3a).

The hairpin *ptf1a* cMO partially impeded pancreatic development even without photoactivation, possibly due to linker degradation or the ability of the reagent to

interconvert between stem-loop and linear forms during the three-day period (Figure 3b). In contrast, the majority of *Tg*(*ptf1a:eGFP*) zygotes injected with the cyclic *ptf1a* cMO developed normally in the absence of UV light (76%, n=21) but failed to form exocrine pancreas upon UV irradiation (95%, n=21) (Figure 3b). Endocrine pancreas development was not affected, as gauged by whole-mount *in situ* hybridization with an antisense probe for *insulin* (Figure 3c). These findings demonstrate the general efficacy of cyclic cMOs and suggest that these chemical tools might be better probes of later embryological processes than hairpin-based reagents.

To conclude these studies, we used the cyclic cMO technology to examine the temporal requirements of *ptf1a* function for exocrine pancreas formation. We uncaged the cyclic *ptf1a* cMO in zebrafish with irradiation conditions optimized for various developmental stages (3 to 52 hpf; Figure S1),. We then assessed exocrine tissue development at 3 dpf by whole-mount *in situ* hybridization with antisense *trypsin* (Figure 4) and *ptf1a* (Figure S2) probes. The resulting expression levels of these exocrine markers followed similar trends, with substantial reductions in transcript levels upon UV irradiation up to 44 hpf. Uncaging of the *ptf1a* cMO at 48 and 52 hpf, however, had only minor effects on their expression. Assuming that cyclic *ptf1a* cMO efficacy is not lost during these studies (MOs can perdure in zebrafish for up to five days[21]), our results suggest that pancreatic cells may be committed to exocrine cell fates as early as 2 dpf.

Taken together, our findings demonstrate the efficacy of cyclic cMOs as reverse-genetic tools for embryological studies and highlight their potential advantages over hairpin-based reagents. Cyclic cMOs can be synthesized in two steps starting from commercially available oligonucleotides, and they can be purified without resorting to HPLC. They also bypass the need for inhibitory oligomers and multiple caging groups. Our results further suggest that these cyclic reagents might be more efficacious than current cMO technologies for studying organogenesis and other late-stage developmental processes. These attributes should facilitate the implementation of cMOs by the developmental biology community and enhance future efforts to decipher embryonic gene function.

References

1. Summerton J, Weller D. Antisense Nucleic Acid Drug Dev. 1997; 7:187–195. [PubMed: 9212909]
2. Heasman J, Kofron M, Wylie C. Dev Biol. 2000; 222:124–134. [PubMed: 10885751]
3. Nasevicius A, Ekker SC. Nat Genet. 2000; 26:216–220. [PubMed: 11017081]
4. Eisen JS, Smith JC. Development. 2008; 135:1735–1743. [PubMed: 18403413]
5. Shestopalov IA, Sinha S, Chen JK. Nat Chem Biol. 2007; 3:650–651. [PubMed: 17717538]
6. Tang X, Maegawa S, Weinberg ES, Dmochowski IJ. J Am Chem Soc. 2007; 129:11000–11001. [PubMed: 17711280]
7. Tomasini AJ, Schuler AD, Zebala JA, Mayer AN. Genesis. 2009; 47:736–743. [PubMed: 19644983]
8. Deiters A, Garner RA, Lusic H, Govan JM, Dush M, Nascone-Yoder NM, Yoder JA. J Am Chem Soc. 2010; 132:15644–15650. [PubMed: 20961123]
9. Tallafuss A, Gibson D, Morcos P, Li Y, Seredick S, Eisen J, Washbourne P. Development. 2012; 139:1691–1699. [PubMed: 22492359]
10. Ouyang X, Shestopalov IA, Sinha S, Zheng G, Pitt CL, Li WH, Olson AJ, Chen JK. J Am Chem Soc. 2009; 131:13255–13269. [PubMed: 19708646]
11. Shestopalov IA, Pitt CLW, Chen JK. Nat Chem Biol. 2012; 8:270–276. [PubMed: 22286130]
12. Ramstein J, Lavery R. Proc Natl Acad Sci U S A. 1988; 85:7231–7235. [PubMed: 3174629]
13. Tang X, Su M, Yu L, Lv C, Wang J, Li Z. Nucleic Acids Res. 2010; 38:3848–3855. [PubMed: 20164090]
14. Halpern ME, Ho RK, Walker C, Kimmel CB. Cell. 1993; 75:99–111. [PubMed: 8402905]

15. Schulte-Merker S, Ho RK, Herrmann BG, Nusslein-Volhard C. Development. 1992; 116:1021–1032. [PubMed: 1295726]

16. Schulte-Merker S, van Eeden FJ, Halpern ME, Kimmel CB, Nusslein-Volhard C. Development. 1994; 120:1009–1015. [PubMed: 7600949]

17. Kawaguchi Y, Cooper B, Gannon M, Ray M, MacDonald RJ, Wright CV. Nat Genet. 2002; 32:128–134. [PubMed: 12185368]

18. Zecchin E, Mavropoulos A, Devos N, Filippi A, Tiso N, Meyer D, Peers B, Bortolussi M, Argenton F. Developmental biology. 2004; 268:174–184. [PubMed: 15031114]

19. Lin JW, Biankin AV, Horb ME, Ghosh B, Prasad NB, Yee NS, Pack MA, Leach SD. Dev Biol. 2004; 270:474–486. [PubMed: 15183727]

20. Pisharath H, Rhee JM, Swanson MA, Leach SD, Parsons MJ. Mech Dev. 2007; 124:218–229. [PubMed: 17223324]

21. Bill BR, Petzold AM, Clark KJ, Schimmenti LA, Ekker SC. Zebrafish. 2009; 6:69–77. [PubMed: 19374550]

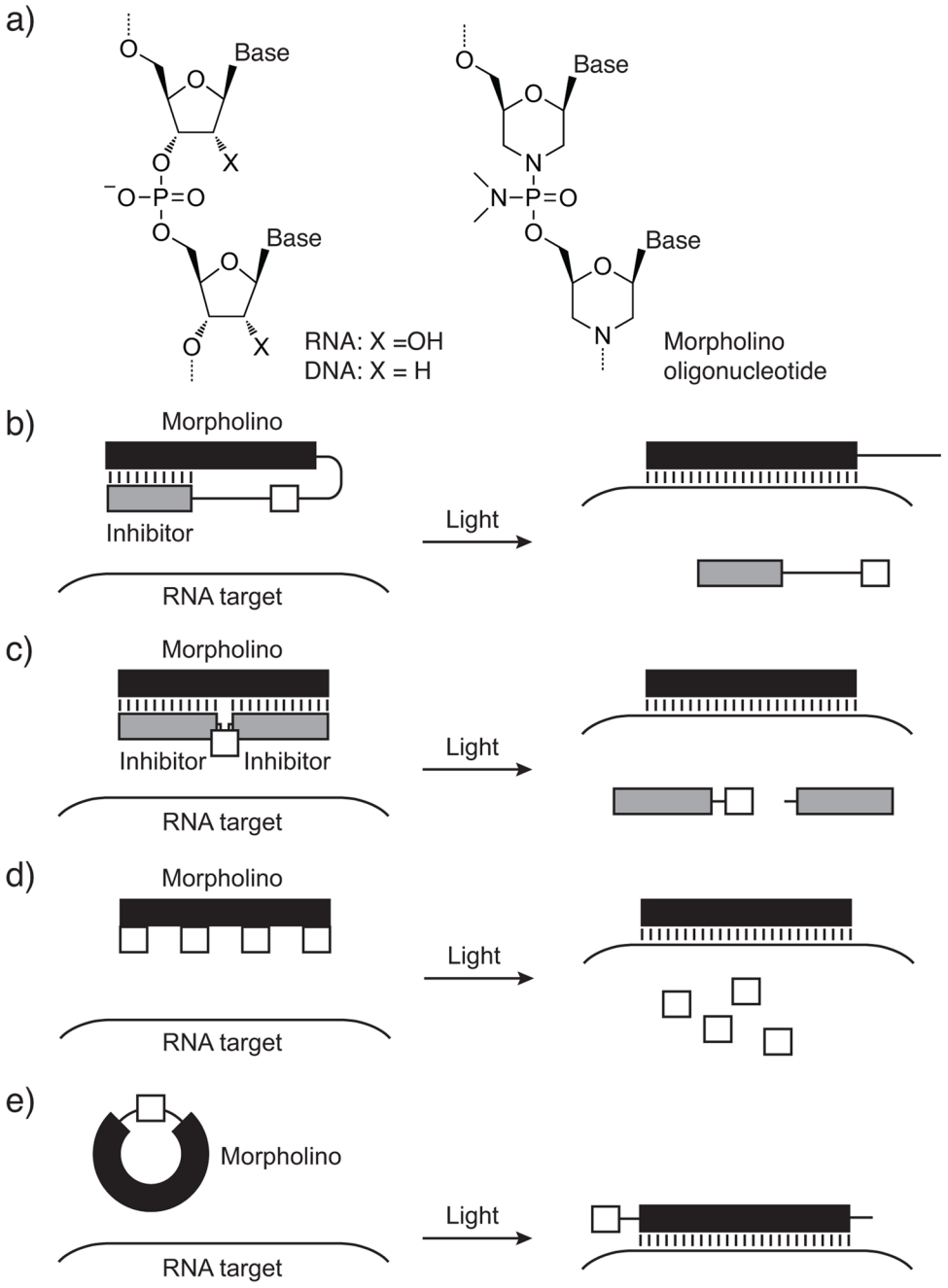

Figure 1.

MOs and their caged derivatives. a) Comparison of DNA/RNA and MO structures. b) Hairpin caged MO. c) MO/caged oligonucleotide duplex. d) MO with caged bases. e) Cyclic caged MO. RNA-targeting MOs are shown in black, inhibitory oligonucleotides in grey, and caging groups in white.

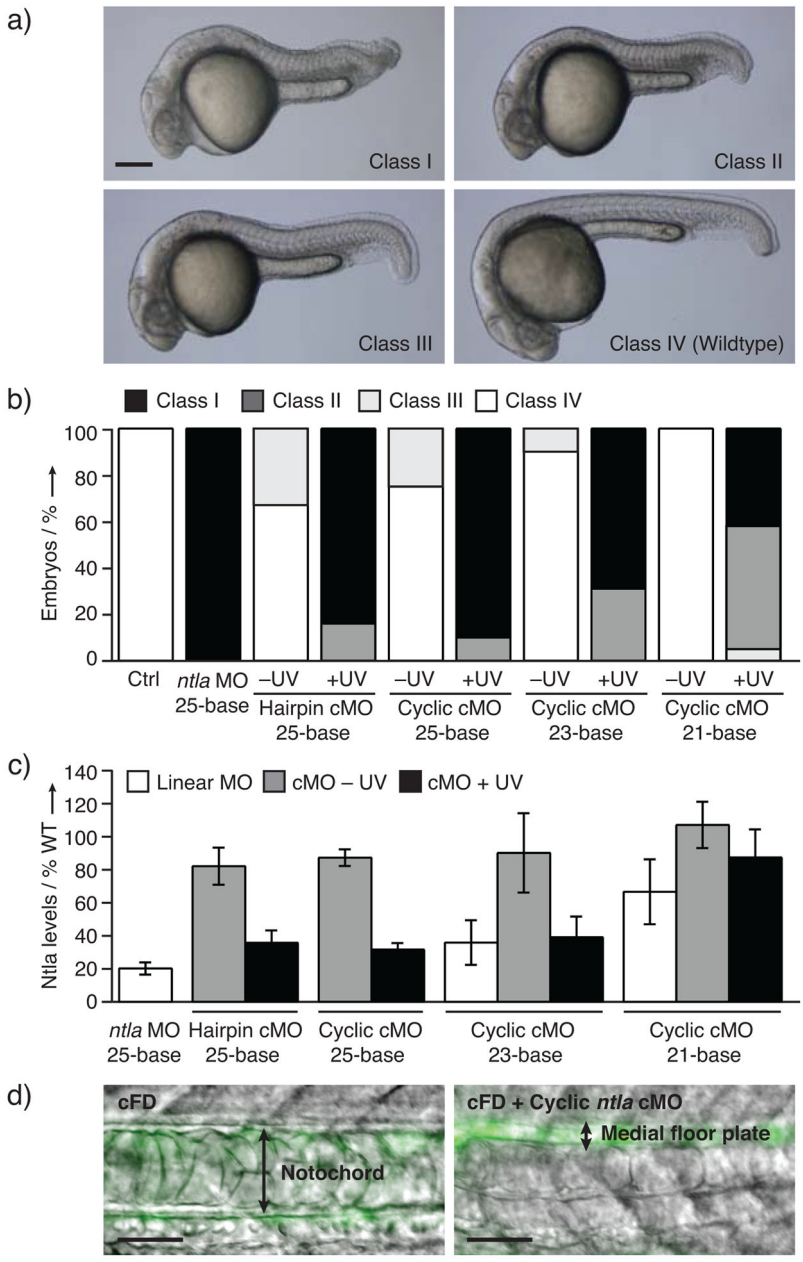

Figure 2.

Comparison of cyclic and hairpin *ntla* cMOs. a) Classification of *ntla* loss-of-function phenotypes. 24-hpf embryos are shown, anterior to the left and dorsal up. Scale bar: 200 μm. b) Phenotypic distributions for embryos injected with the indicated reagents and either cultured in the dark or globally UV irradiated at 3 hpf. Between 13 and 24 embryos were analyzed for each condition. c) Ntla protein levels in 10-hpf embryos subjected to the indicated conditions. Data are the average of at least 4 experiments (6 embryos/condition) ± s.e.m., normalized with respect to β-actin. d) Phenotypes observed in embryos injected with caged fluorescein-conjugated dextran (cFD) ± the cyclic *ntla* cMO and irradiated within the shield at 6 hpf. Trunk regions of 36-hpf embryos are shown as overlays of differential interference contrast (DIC) and fluorescence micrographs (anterior left, dorsal up). Scale bars: 50 μm.

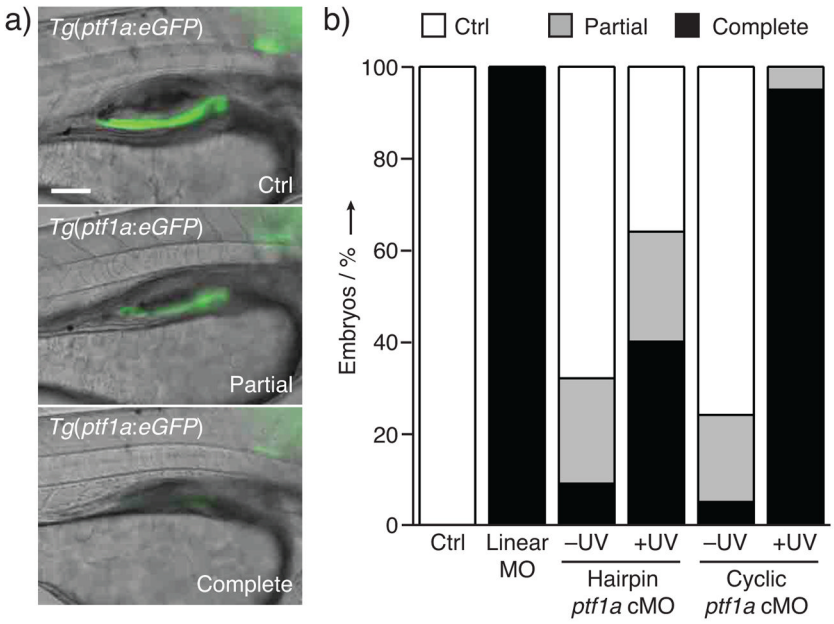

Figure 3.

Comparison of cyclic and hairpin *ptf1a* cMOs. a) Classification of *ptf1a* loss-of-function phenotypes according to pancreas-specific eGFP expression in *Tg*(*ptf1a:eGFP*) zebrafish. Fluorescence micrographs of 3-dpf larvae are shown, anterior to the right and dorsal up. Scale bar: 100 μm. b) Phenotypic distributions for embryos injected with the indicated reagents and either cultured in the dark or globally UV irradiated at 3 hpf. Between 21 and 31 embryos were analyzed for each condition.

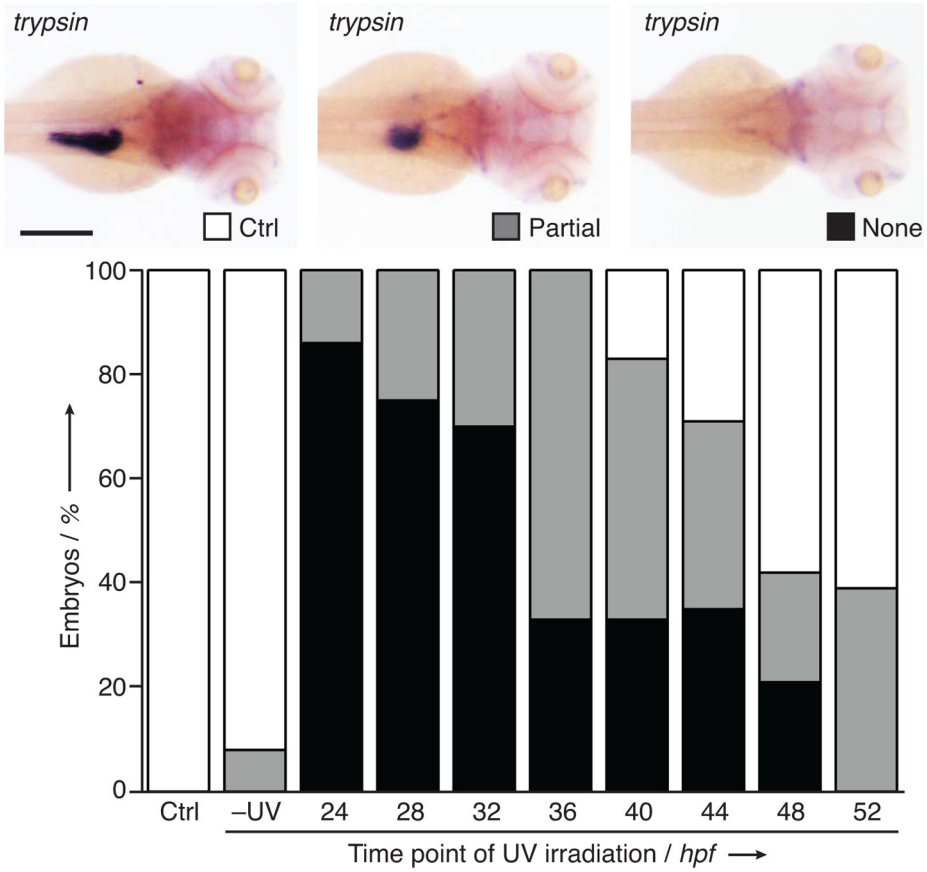

Figure 4.

Temporal analysis of *ptf1a*-dependent exocrine pancreas development. Classification of *trypsin* expression levels and phenotypic distributions observed for embryos injected with the cyclic *ptf1a* cMO and either cultured in the dark or globally UV irradiated at the designated time points. Dorsal views of 3-dpf larvae are shown, anterior to the right. Scale bar: 200 μm.

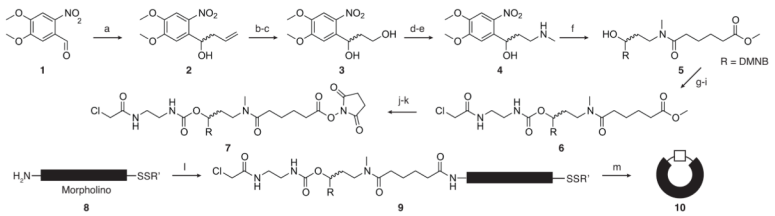

Scheme 1.

Cyclic *ntla* cMO synthesis. a) allyl TMS, $TiCl_4$, CH_2Cl_2, 98%; b) O_3, MeOH; c) $NaBH_4$, MeOH, 74% over 2 steps; d) TsCl, pyridine, 63%; e) methylamine, THF, 87%; f) methyl adipoyl chloride, DIPEA, CH_2Cl_2, 57%; g) 1,1′-carbonyl diimidazole, CH_2Cl_2; h) ethylenediamine, CH_2Cl_2; i) 2-chloroacetyl chloride, Et_3N, CH_2Cl_2, 54% over 3 steps; j) LiOH, THF, H_2O; k) *N*,*N*′-disuccinimidyl carbonate, pyridine, CH_3CN, 68% over 2 steps; l) 5′-amine, 3′-alkyl disulfide *ntla* MO (21-, 23-, or 25-base), 0.1 M $Na_2B_4O_7$ pH 8.5, DMSO, 69–95%; m) TCEP resin, 0.1 M Tris-HCl buffer, pH 8.4, 84–92%.

Table 1

Thermodynamic parameters of MO/RNA duplexes

MO oligomer[a]	T_m (°C) linear[b]	ΔG (kcal/mol) linear[b]	T_m (°C) cyclic [b]	ΔG (kcal/mol)cyclic[b]	ΔT_m (°C)[c]	ΔΔG (kcal/mol)[c]
25-base	78.3 ± 0.9	−22.1 ± 2.3	75.2 ± 1.2	−18.5 ± 0.7	3.1 ± 0.7	3.6 ± 0.9
23-base	77.0 ± 2.0	−20.4 ± 2.0	68.7 ± 1.3	−15.9 ± 1.0	8.3 ± 0.9	4.5 ± 0.9
21-base	74.2 ± 1.3	−19.7 ± 1.1	60.2 ± 1.3	−14.0 ± 0.4	14.0 ± 1.1	5.7 ± 0.7

[a] See Table S1 for sequence information.

[b] Average values of 3–12 experiments ± s.d.

[c] Absolute differences between linear MO/RNA and cyclic MO/RNA duplexes ± s.e.